

Reverse Shocks in the Relativistic Outflows of Gravitational Wave Detected Neutron Star Binary Mergers

Gavin P. Lamb¹★ and Shiho Kobayashi,²

¹*Department of Physics and Astronomy, University of Leicester, University Road, Leicester, LE1 7RH, UK*

²*Astrophysics Research Institute, Liverpool John Moores University, IC2, Liverpool Science Park, 146 Brownlow Hill, Liverpool, L3 5RF, UK*

Accepted XXX. Received YYY; in original form ZZZ

ABSTRACT

The afterglows to gamma-ray bursts (GRBs) are due to synchrotron emission from shocks generated as an ultra-relativistic outflow decelerates. A forward and a reverse shock will form, however, where emission from the forward shock is well studied as a potential counterpart to gravitational wave detected neutron star mergers the reverse shock has been neglected. Here, we show how the reverse shock contributes to the afterglow from an off-axis and structured outflow. The reverse shock will be observable as a brightening feature in the rising afterglow at radio frequencies for bursts at < 100 Mpc and systems inclined $\lesssim 30^\circ$ (or ~ 5 times the core opening angle) at $\sim 1 - 10$ days post-merger. For structured outflows, enhancement of the reverse shock emission by a strong magnetic field within the outflow is required for the emission to dominate the afterglow at early times. Early radio photometry/polarimetry of the reverse shock could reveal the presence of a strong magnetic field associated with the merger remnant.

Key words: gamma-ray burst: general – gravitational waves – stars: neutron

1 INTRODUCTION

The structure of the outflows that drive the shock system responsible for gamma-ray burst (GRB) afterglows is well discussed in the literature (e.g. Rossi, Lazzati & Rees 2002; Panaiteescu 2005; Granot 2005; Salafia, Ghisellini, Pescalli, Ghirlanda & Nappo 2015). Due to the highly beamed nature of GRBs, observations of the afterglow are typically limited to cases where the inclination of the system is small and the wider structure of the outflow remains hidden. However, attempts have been made at interpreting the observational evidence to support various outflow structures in GRBs (e.g. Takami, Yamazaki, Sakamoto & Sato 2007; Pescalli, Ghirlanda, Salafia, Ghisellini, Nappo & Salvaterra 2015; Beniamini & Nakar 2019). Gravitational wave (GW) detected mergers involving at least one neutron star will typically be seen off the central rotational axis and will act as a probe for the structure of the jet or outflow that is likely responsible for the cosmological population of short-duration GRBs (Lamb & Kobayashi 2017; Lazzati, Deich, Morsony & Workman 2017; Jin, et al. 2018; Kathirgamaraju, Barniol Duran & Giannios 2018). Following the observation via GW of the binary neutron star merger GW170817 (Abbott, et al. 2017), and year-long observations of the evolving afterglow, constraints on the structure of the afterglow driving outflow for

this event have been made (e.g. Gill & Granot 2018; Lamb & Kobayashi 2018; Lazzati, et al. 2018; Lyman, et al. 2018; Margutti, et al. 2018; Resmi, et al. 2018; Troja, et al. 2018; van Eerten, et al. 2018; Kathirgamaraju, Tchekhovskoy, Giannios & Barniol Duran 2019; Lamb, et al. 2019).

The afterglow estimates for structured outflows have so far ignored the contribution of a reverse shock. Reverse shocks (e.g. Mészáros & Rees 1997; Sari & Piran 1999; Kobayashi 2000; Kobayashi & Sari 2000; Resmi & Zhang 2016) have been identified in the afterglows to long GRBs and should accompany short GRBs, although they have been difficult to detect (Lloyd-Ronning 2018). However, in favourable circumstances, they should contribute to the observable afterglow at radio frequencies to GW triggered events. Here we show how the phenomenology of the reverse shock emission can be used as a probe for the magnetisation of the central engine and potentially assist in identifying the likely outflow structure.

Constraints on the structure of short-duration GRB outflows have been found following GW170817. These constraints include: a narrow jet and high core energy for jet outflows in mergers (Beniamini, Petropoulou, Barniol Duran & Giannios 2019), and a Lorentz-factor for the wider components or cocoon ≥ 5 or ~ 10 for the cocoon shock breakout scenario (e.g. Xie, Zrake & MacFadyen 2018; Beloborodov, Lundman & Levin 2018; Fraija, Pedreira & Veres 2019; Matsumoto, Nakar & Piran 2019). We use these con-

★ E-mail: gpl6@le.ac.uk

straints to limit the outflow structure profiles for our reverse shock estimation.

In § 2 we discuss the classical reverse shock scenario and in § 2.1 apply the method to the structured outflow models used to produce light-curves for afterglows observed at any inclination. In § 2.2 we briefly discuss the case of a relativistic cocoon. In § 3 we discuss our results and in § 4 we give final remarks and conclusions.

2 METHOD: THE REVERSE SHOCK

Using the method for determining the afterglow emission from a structured relativistic outflow in Lamb & Kobayashi (2017), with the dynamical evolution and expansion description in Lamb, Mandel & Resmi (2018) we include synchrotron self-absorption (as in Lamb, et al. 2019, and described below) and add a description for the reverse shock in these systems. For the reverse shock we follow Kobayashi (2000); Kobayashi & Sari (2000); Harrison & Kobayashi (2013) and use the dynamical evolution of the blast-wave to scale the reverse shock peak conditions.

The behaviour of the emission from a reverse shock depends, primarily, on the width of the shell through which the shock propagates. The width of the shell Δ_0 is an unknown free-parameter, although usually assumed to be the product of the speed-of-light c and the GRB duration, giving two cases; a thick shell, where $\Delta_0 > l/2\Gamma_0^{8/3}$ or thin shell with $\Delta_0 < l/2\Gamma_0^{8/3}$; here, $l = (3E_k/4\pi n m_p c^2)^{1/3}$ is the Sedov length and Γ_0 is the coasting phase bulk Lorentz factor of the outflow (Kobayashi, Piran & Sari 1999), E_k is the isotropic equivalent kinetic energy of the blast-wave, n the ambient number density of protons in the surrounding medium, and m_p the mass of a proton. Short GRBs are typically described by the thin shell case.

The synchrotron emission with spectral regime is estimated following Sari, Piran & Narayan (1998); Wijers & Galama (1999). For a reverse shock in the thin shell case, Kobayashi (2000) demonstrated that the spectral peak flux $F_{\max,r}$, the characteristic frequency $\nu_{m,r}$ and the cooling frequency $\nu_{c,r}$, scale with observed time as $F_{\max,r} \propto t^{3/2}$, $\nu_{m,r} \propto t^6$, and $\nu_{c,r} \propto t^{-2}$ where $t < t_d$; and $F_{\max,r} \propto t^{-34/35}$, $\nu_{m,r} \propto t^{-54/35}$, and $\nu_{c,r} \propto t^{4/35}$ where $t > t_d$. Here t_d is the deceleration time for the outflow in the observers frame.

For the reverse shock the values of $F_{\max,r}$, $\nu_{m,r}$, t_d vary from early analytic estimates via a factor that depends on the dimensionless parameter ξ_0 , where $\xi_0 = (l/\Delta_0)^{1/2}\Gamma_0^{-4/3}$ (Sari & Piran 1995). The correction factors for $F_{\max,r}$ and $\nu_{m,r}$ are defined here as $F_{\max,r}(t_d)/F_{\max,f}(t_d) = \Gamma_0 C_F$, and $\nu_{m,r}(t_d)/\nu_{m,f}(t_d) = \Gamma_0^{-2} C_m$, and the observed deceleration time $t_d = C_t l/c \Gamma_0^{8/3}$. These correction factors can be approximated as $C_F \sim (1.5 + 5\xi_0^{-1.3})^{-1}$, $C_m \sim (10^{-2.3} + \xi_0^{-3})$, and $C_t \sim 0.2 + \xi_0^{-2}$ respectively (Harrison & Kobayashi 2013). As the reverse shock probes the shell material towards the central engine that is driving the outflow, a strong magnetic field associated with the engine will further enhance the reverse shock parameters by a factor $R_B^{1/2}$ for both $F_{\max,r}$ and $\nu_{m,r}$, and by the factor $R_B^{-3/2}$ for $\nu_{c,r}$; here $R_B \equiv \varepsilon_{B,r}/\varepsilon_{B,f}$ where ε_B is the magnetic microphysical parameter and the subscript f or r refers to forward- or reverse-shock respec-

tively (Zhang, Kobayashi & Mészáros 2003; Gomboc, et al. 2008). Very high values of R_B have been obtained for some long GRBs (Zhang, Kobayashi & Mészáros 2003; Harrison & Kobayashi 2013; Huang, et al. 2016).

At an inclination ι that is outside of the jet half opening angle θ_j , then due to geometric considerations, the observed flux is $F_\nu = F_{\nu,o}(\delta/\delta_0)^k$, where $[\iota - \theta_j] > 0$ then $\delta = 1/\Gamma(1 - \beta \cos[\iota - \theta_j])$ is the relativistic Doppler factor and $\beta = (1 - \Gamma^{-2})^{1/2}$, and the subscript ‘o’ indicates the on-axis value $\delta_0 = 1/\Gamma(1 - \beta)$. The value of k depends on the separation from the jet edge with $k \sim 2$ for $\iota \lesssim 2\theta_j$ and $k \sim 3$ for $\iota \gtrsim 2\theta_j$ (Ioka & Nakamura 2018). For an outflow with angular structure¹ we sum the evaluated flux from each angular segment across the outflow.

At low frequencies synchrotron self-absorption (SSA) becomes important. SSA limits the flux for the reverse shock more efficiently than for the forward shock due to the lower effective temperature of the electrons in the reverse-shock region. The limiting flux, at a given frequency ν and observer time t , in the reverse shock can be estimated by considering the intensity of a black-body with the reverse shock temperature (e.g. Kobayashi & Sari 2000). Alternatively, see Resmi & Zhang (2016) where they consider the opacity of the source to estimate the SSA limit.

2.1 Reverse shocks viewed off-axis

To determine if the signature of a reverse shock is apparent in the afterglow from a GW detected merger jet we estimate the flux from a variety of outflow structures with a range of inclinations. Following Lamb & Kobayashi (2017) we consider four jet structures generally described as a top-hat, two-component, power-law, and a Gaussian. The top-hat model is a jet with a uniform kinetic energy and velocity distribution and sharp edges at the value θ_c used as the core angular width for the jets with a more complex angular structure. The two-component model follows Lamb, et al. (2019) with a top-hat jet surrounded by a second component with 10% of the core isotropic equivalent energy and a Lorentz factor of 5. For the power-law model we follow Lamb & Kobayashi (2017) where outside of a top hat core the energy and Lorentz factor scale with angle as $\propto (\theta/\theta_c)^{-2}$, and a condition ensuring $\Gamma \geq 1$. The Gaussian model follows the description in Lamb & Kobayashi (2018); Resmi, et al. (2018); Lamb, et al. (2019); $E(\theta) = E_c e^{-\theta^2/\theta_c^2}$ and $\Gamma(\theta) = (\Gamma_{0,c} - 1) e^{-\theta^2/2\theta_c^2} + 1$, where the subscript ‘c’ indicates the central or core values. For all the structured jets we limit the structure by imposing an edge at $\theta_j = 15^\circ$.

We fix various fiducial parameters for the jets with the core, or central values, as $E = 10^{51}$ erg (or 10^{52} erg for the Gaussian model), $\Gamma_0 = 100$, and $\theta_c = 6^\circ$. The other model parameters are; the electron distribution index $p = 2.2$, the microphysical parameters $\varepsilon_{B,f} = \varepsilon_e^2 = 10^{-2}$, and the ambient density $n = 10^{-3}$ cm⁻³.

Fig. 1 shows the afterglow light-curves, observed at 3 GHz and inclinations $\iota = [0, 2\theta_c, 3\theta_c, 6\theta_c, 9\theta_c, 12\theta_c, 15\theta_c]$,

¹ Angular structure refers to an outflow with energy and/or Lorentz factor that vary with angular separation from the central axis; $[E_k(\theta), \Gamma_0(\theta)] \propto f(\theta)$

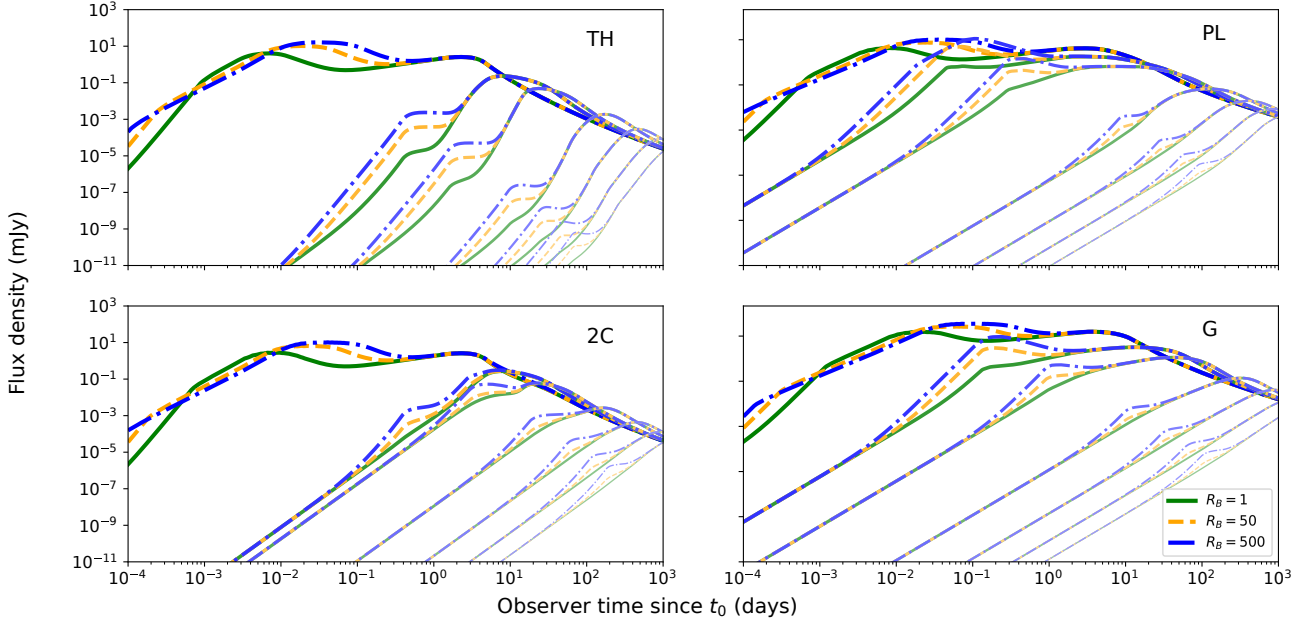


Figure 1. Jet structure afterglows at a distance 100 Mpc and observed in radio at 3 GHz. Afterglows are viewed at $[0, 12, 18, 36, 54, 72, 90]^\circ$ where the line thickness and boldness scale with the inclination. Three magnetization parameters are shown, $R_B = [1, 50, 500]$, solid green, dashed orange, and dash-dotted blue line respectively. The four structure models are as described in the text: top left – ‘top hat’ (TH); bottom left – two-component (2C); top right – power-law (PL); bottom right – Gaussian (G). The x -axis shows the time since t_0 – either, a GRB trigger for an on-axis case, or a GW trigger when off-axis. The reverse shock is seen as an early peak when on-axis and during the rising phase when viewed off-axis.

for the four jet structure models considered². The reverse shock, in each case, peaks for an on-axis observer at $t \sim 0.001 - 0.1$ days. The second peak at $\sim 1 - 10$ days is the forward shock afterglow. Off-axis, the reverse shock is expected to contribute before the afterglow peak time – although, in the case of a complex structure, the reverse shock may still be bright, creating a two peaked afterglow, even for observers at inclinations greater than the jet core opening angle.

The on-axis afterglows in Fig. 1 show the reverse shock is self-absorbed before the peak time in all cases i.e. $F_{BB} < F_\nu$, here F_{BB} is the flux limit for SSA. For the $R_B = 1$ case, the transition from un-absorbed to SSA can be seen by the change in the temporal index at ~ 0.001 days. A flattening in the SSA light-curve indicates the passage of the characteristic frequency $\nu_{m,r} < \nu$. Off-axis, the SSA emission has a limited contribution (effects can be seen for the power-law structured case where the magnetization is high and the system mildly inclined $\iota = 12^\circ$).

For the top-hat jet (TH), top-left in Fig. 1, the off-axis reverse shock emission results in a brightening feature in the rising afterglow. For a magnetized ejecta where $R_B > 1$ this feature is present at all inclinations.

The two-component (2C), shown bottom-left in Fig. 1, shows similar features to the TH case. However, at higher inclinations, the forward shock emission from the low- Γ wide component competes with the off-axis emission from a re-

verse shock in the jet core. A reverse shock in the wider component is faint and only appears brighter than the forward shock afterglow where $R_B > 1$. At higher inclinations, the reverse shock emission from the low- Γ wide/second component results in an afterglow that rapidly rises to a plateau, for $R_B = 500$, before the forward shock emission from the energetic core dominates resulting in a late-time peak.

The right panels in Fig. 1 show the afterglow light-curves for a power-law (PL) and a Gaussian structured (G) jet (top and bottom respectively). Phenomenologically, these two cases appear similar; the smooth change in the energy and Lorentz factor profile means that, overall, afterglow emission is brighter for longer for an off-axis observer than for a regular top-hat jet – this is consistent with the findings of Lamb, Tanaka & Kobayashi (2018) where orphan afterglows from structured jets have a higher rate of two or more detections with typical survey telescope cadences. However, for a power-law structure the reverse shock, both on- and off-axis, is broader than for a Gaussian structure. For the Gaussian jet, the energy drops very rapidly with angle outside of the jet core when compared to the power-law case and so the contribution to the afterglow emission from the wider angled components is significantly reduced. The reverse shock for the highly magnetized cases are observable above the forward shock, even at high inclinations. For both the power-law and Gaussian structured jets, observed at mild inclinations $\iota \sim (2 - 3)\theta_c$ (up to $\sim 6\theta_c$ for the Gaussian case), the reverse shock peak typically coincides with the start of the shallow incline to peak.

² We do not consider the counter-jet here and therefore the flux density at $\sim 90^\circ$, or our $15\theta_c$, will be brighter by a factor 2 where the counter-jet is identical to the forward jet

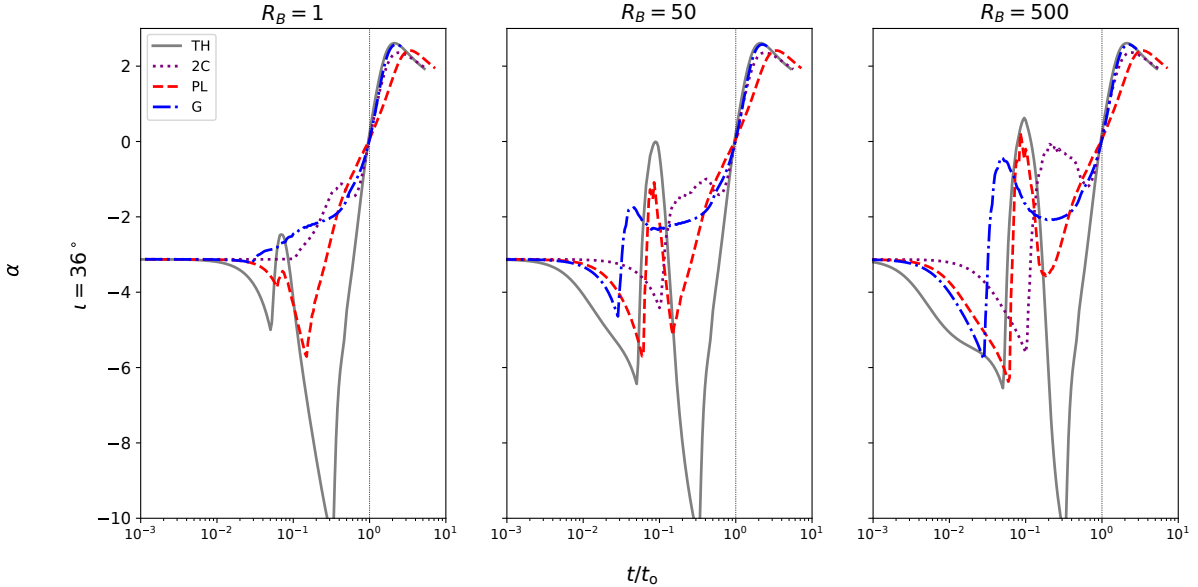


Figure 2. The rise index α defined as $F \propto t^{-\alpha}$ for the 3 GHz afterglow light-curves at an inclination $\iota = 36^\circ$ or $6\theta_c$. The x -axis shows time normalised to t_0 , the observed light-curve peak due to emission from the forward shock, the vertical line at $t/t_0 = 1$. Each column shows a single magnetic parameter, $R_B = [1, 50, 500]$ respectively. The jet structures are indicated by the line colour and style: TH – top-hat with a solid grey line; 2C – two-component with a dotted purple line; PL – power-law with a dashed red line; and G – Gaussian with a blue dashed-dotted line.

2.2 Reverse shocks in cocoons

A jet that stalls as it drills through the envelope of material ejected during the merger process will inflate a cocoon of energised matter (Gottlieb, Nakar & Piran 2018). As the cocoon material propagates into the surrounding medium it will sweep up material in the same fashion as a GRB jet, generating a shock system that will produce a broadband afterglow. For such a cocoon of material, with a relativistic velocity distribution, the slower components will catch up and refresh the forward shock creating a distinctive, slow rising afterglow (e.g. Mooley, et al. 2018). Although the afterglow following GRB 170817A was not due to such a choked-jet system, such transients may exist and the electromagnetic counterparts to future GW detected mergers may reveal the afterglow to a choked-jet cocoon. The existence of such a choked-jet population is supported by the duration analysis of short-duration GRBs (Moharana & Piran 2017).

The afterglow from a wide-angled choked-jet system will be semi-isotropic, depending on the initial opening angle of the outflow $\theta \sim 30 - 40^\circ$ (Nakar, Gottlieb, Piran, Kasliwal & Hallinan 2018), and potentially bright on long timescales (~ 100 s days) for nearby events where the cocoon has a radial velocity distribution (Fraija, Pedreira & Veres 2019). A reverse shock will travel back into the cocoon and the forward shock will be continuously refreshed and energised. The reverse shock probes the slower material catching and energising the forward shock system. While slower material continues to refresh the forward shock, the reverse shock will persist.

The maximum synchrotron flux from a reverse shock for a cocoon with a uniform energy distribution and a fastest

component with $\Gamma_0 = 10$ will be $F_{\max,r} \sim R_B^{1/2} \Gamma_0 C_F F_{\max,f}$; in the thin shell regime when $\Delta_0 \downarrow 0$ then $C_F \rightarrow 0.667$. Similarly, the coefficient for the characteristic frequency $\nu_{m,r}$ is $C_m \rightarrow 5 \times 10^{-3}$. As the slower components refresh the system, the relevant Lorentz factor Γ_0 for the reverse shock will reduce – $F_{\max,r}$ and $\nu_{m,r}$ depend on the Lorentz factor as Γ_0 and Γ_0^2 respectively.

For the fastest component, the forward shock will have a characteristic frequency $\nu_m \sim 3.2 \times 10^{10}$ Hz, then the peak synchrotron frequency for the reverse shock is $\sim 1.6 \times 10^6$ Hz; assuming slow cooling, the flux at ~ 3 GHz would be a factor ~ 0.07 of the peak forward shock flux at t_d . For a velocity distribution within the cocoon that ranges from $\Gamma = 10 - 1.4$, then as the forward shock is energised, where $E(> \Gamma\beta) \propto (\Gamma\beta)^{-\kappa}$ here $4.5 \leq \kappa \leq 6.2$ (Nakar & Piran 2018), and $F_{\max,f} \propto E$ the forward shock emission will always dominate over that from the reverse shock which propagates into a shell with the lower initial energy.

In the case where the cocoon is magnetized, the reverse shock for our parameters will initially dominate over the forward shock when $R_B \gtrsim 26$. Where the initial Lorentz factor of the outflow is < 10 the required R_B increases e.g. for $\Gamma_0 = 5$, then $R_B \gtrsim 180$. As the forward shock is energised, the emission from the reverse shock will be buried beneath that from the forward shock. In such a case, the signature of a reverse shock, will appear as a radio flare at $\sim t_d$ for the outflow.

3 DISCUSSION

By considering a reverse shock for various jet or outflow structures, we have shown that the pre-peak afterglow for an off-axis observer will contain a distinctive feature with a reverse shock origin. A larger residual magnetic field from the central engine will enhance the reverse shock emission, and for small inclinations, may result in the brightest afterglow peak when observed at low-frequencies.

For the thin shell case of short-duration GRBs, the low characteristic frequency and the early peak time for the reverse-shock emission means that fast response and deep radio frequency photometry of GW triggered neutron star mergers is critical in identifying the reverse shock contribution. At a distance of 100 Mpc, where a system is inclined $\iota < 20^\circ$ the reverse shock feature will appear on a timescale $t \sim 1 - 10$ days post merger and at a 3 GHz flux density of $F_\nu > 10^{-2} \mu\text{Jy}$ for a top-hat jet and $F_\nu > 10 \mu\text{Jy}$ for a structured jet or outflow.

Our example in Fig. 1, shows that for an observer at the typical GW detected inclination of $\sim 38^\circ$ (Lamb & Kobayashi 2017), the flux density is $\sim 10^{-5} \mu\text{Jy}$ for a top-hat jet with an opening angle of 6° . For the structured outflows a magnetization parameter $R_B > 1$ is required. Where this is the case, the flux density is $\sim 1 \mu\text{Jy}$. Observations at this level will be difficult, however, as the afterglow brightens the changing temporal index of the rising afterglow will reveal the reverse shock, see Fig. 2. Variability in the rise index for the afterglow at higher inclinations shows the contribution from the reverse shock in the jet core.

In Fig. 2, the rise index evolution with time before the afterglow forward shock peak is shown for an observer at $\iota = 36^\circ = 6\theta_c$. Where $R_B = 1$, the reverse shock can be seen for the top-hat³ and marginally for the power-law case at $t/t_0 \sim 10^{-1}$. Whereas for the two-component and Gaussian models, the rise index gradually flattens to the peak at $\alpha = 0$ as expected from a forward shock. For higher values of R_B , the reverse shock is more obvious – briefly steepening the incline at $t/t_0 \lesssim 10^{-1}$ before a shallower rise before becoming forward shock dominated and peaking at $t/t_0 = 1$. Early radio emission for the afterglow to GW170817 could indicate the existence of a short lived reverse shock component (Lamb et al. in prep).

For short GRBs at cosmological distances, the afterglow is expected to be at small inclinations within the jet opening angle or the core angle for a structured jet. From Fig. 1 it is clear that on-axis the different structures show little difference – note that the power-law case has a slightly broadened forward shock peak and never declines as steeply as the other examples. This is due to the choice of power-law index in the

³ The steep rise to peak in the top-hat case, and the peak duration for the off-axis observed afterglow is likely an effect of the afterglow approximation. Where the full density profile of the forward shock is considered, the rise-time is earlier and the peak is broadened (e.g. van Eerten, van der Horst & MacFadyen 2012; De Colle, Granot, López-Cámarra & Ramirez-Ruiz 2012). 2D hydrodynamic simulations have shown that the afterglow from a top-hat jet, when observed off-axis, will look more like a structured outflow (Gill, Granot, De Colle & Urrutia 2019). In such a case, we expect the reverse shock to appear similar to the case of an angular structured outflow shown here

structure description, where the components outside of the jet core remain energetic to the edge at 15° . However, for untriggered transient surveys such as the Square Kilometre Array, the increased duration for a structured outflow with a reverse shock will increase the likelihood of making multiple detections of an orphan afterglow at higher distances. For optical transient surveys such as the Large Synoptic Survey Telescope, the reverse shock is not expected to be bright and the transient rate estimated from forward shock considerations will remain unaffected by inclusion of a reverse shock (e.g. Lamb, Tanaka & Kobayashi 2018).

4 CONCLUSIONS

For mildly inclined $\iota \lesssim 30^\circ$ GW detected binary neutron star mergers within ~ 100 Mpc, the reverse shock will show a distinct feature in the rising afterglow emission at $1 - 10$ days post-merger. For structured outflows described by a power-law or Gaussian profile, the reverse shock will appear as an early bump or plateau before a gradual rise to peak at ~ 100 days. The flux density level of the reverse shock can be used to estimate the degree of magnetization within the outflow ejecta. This magnetization is likely due to the central engine where strong magnetic fields are expected during the launch and acceleration of a relativistic outflow.

ACKNOWLEDGEMENTS

GPL is supported by STFC grant ST/N000757/1.

REFERENCES

- Abbott B. P., et al., 2017, *PhRvL*, 119, 161101
- Beloborodov A. M., Lundman C., Levin Y., 2018, arXiv e-prints, arXiv:1812.11247
- Beniamini P., Petropoulou M., Barniol Duran R., Giannios D., 2019, *MNRAS*, 483, 840
- Beniamini P., Nakar E., 2019, *MNRAS*, 482, 5430
- D'Avanzo P., et al., 2018, *A&A*, 613, L1
- De Colle F., Granot J., López-Cámarra D., Ramirez-Ruiz E., 2012, *ApJ*, 746, 122
- Fraija N., Pedreira A. C. C. do E. S., Veres P., 2019, *ApJ*, 871, 200
- Gill R., Granot J., 2018, *MNRAS*, 478, 4128
- Gill R., Granot J., De Colle F., Urrutia G., 2019, arXiv e-prints, arXiv:1902.10303
- Gomboc A., et al., 2008, *ApJ*, 687, 443
- Gottlieb O., Nakar E., Piran T., 2018, *MNRAS*, 473, 576
- Granot J., 2005, *ApJ*, 631, 1022
- Harrison R., Kobayashi S., 2013, *ApJ*, 772, 101
- Huang X.-L., et al., 2016, *ApJ*, 833, 100
- Ioka K., Nakamura T., 2018, *PTEP*, 2018, 043E02
- Jin Z.-P., et al., 2018, *ApJ*, 857, 128
- Kathirgamaraju A., Barniol Duran R., Giannios D., 2018, *MNRAS*, 473, L121
- Kathirgamaraju A., Tchekhovskoy A., Giannios D., Barniol Duran R., 2019, *MNRAS*, 484, L98
- Kobayashi S., Piran T., Sari R., 1999, *ApJ*, 513, 669
- Kobayashi S., 2000, *ApJ*, 545, 807
- Kobayashi S., Sari R., 2000, *ApJ*, 542, 819
- Lamb G. P., Kobayashi S., 2017, *MNRAS*, 472, 4953
- Lamb G. P., Kobayashi S., 2018, *MNRAS*, 478, 733

Lamb G. P., Mandel I., Resmi L., 2018, MNRAS, 481, 2581
 Lamb G. P., Tanaka M., Kobayashi S., 2018, MNRAS, 476, 4435
 Lamb G. P., et al., 2019, ApJ, 870, L15
 Lazzati D., Deich A., Morsony B. J., Workman J. C., 2017, MNRAS, 471, 1652
 Lazzati D., et al., 2018, PhRvL, 120, 241103
 Lloyd-Ronning N., 2018, Galax, 6, 103
 Lyman J. D., et al., 2018, Nature Astronomy, 2, 751
 Margutti R., et al., 2018, ApJ, 856, L18
 Matsumoto T., Nakar E., Piran T., 2019, MNRAS, 483, 1247
 Mészáros P., Rees M. J., 1997, ApJ, 476, 232
 Moharana R., Piran T., 2017, MNRAS, 472, L55
 Mooley K. P., et al., 2018, Natur, 554, 207
 Nakar E., Gottlieb O., Piran T., Kasliwal M. M., Hallinan G., 2018, ApJ, 867, 18
 Nakar E., Piran T., 2018, MNRAS, 478, 407
 Panaiteescu A., 2005, MNRAS, 362, 921
 Pescalli A., Ghirlanda G., Salafia O. S., Ghisellini G., Nappo F., Salvaterra R., 2015, MNRAS, 447, 1911
 Resmi L., Zhang B., 2016, ApJ, 825, 48
 Resmi L., et al., 2018, ApJ, 867, 57
 Rossi E., Lazzati D., Rees M. J., 2002, MNRAS, 332, 945
 Salafia O. S., Ghisellini G., Pescalli A., Ghirlanda G., Nappo F., 2015, MNRAS, 450, 3549
 Sari R., Piran T., 1995, ApJ, 455, L143
 Sari R., Piran T., Narayan R., 1998, ApJ, 497, L17
 Sari R., Piran T., 1999, ApJ, 520, 641
 Takami K., Yamazaki R., Sakamoto T., Sato G., 2007, ApJ, 663, 1118
 Troja E., et al., 2018, MNRAS, 478, L18
 van Eerten H., van der Horst A., MacFadyen A., 2012, ApJ, 749, 44
 van Eerten E. T. H., et al., 2018, arXiv e-prints, arXiv:1808.06617
 Wijers R. A. M. J., Galama T. J., 1999, ApJ, 523, 177
 Xie X., Zrake J., MacFadyen A., 2018, ApJ, 863, 58
 Zhang B., Kobayashi S., Mészáros P., 2003, ApJ, 595, 950

This paper has been typeset from a *TeX/LaTeX* file prepared by the author.